Vibrational relaxation pathways of AI and AII modes in N-methylacetamide.

L. Piatkowski[1, a)] and H. J. Bakker[1]

FOM Institute AMOLF, Science Park 104, 1098 XG Amsterdam,

The Netherlands

We studied the vibrational energy relaxation mechanisms of the amide I and amide II modes of N-methylacetamide (NMA) monomers dissolved in bromoform using polarization-resolved femtosecond two-color vibrational spectroscopy. The results show that the excited amide I vibration transfers its excitation energy to the amide II vibration with a time constant of 8.3 ± 1 ps. In addition to this energy exchange process, we observe that the excited amide I and amide II vibrations both relax to a final thermal state. For the amide I mode this latter process dominates the vibrational relaxation of this mode. We find that the vibrational relaxation of the amide I mode depends on frequency which can be well explained from the presence of two subbands with different vibrational lifetimes ($\sim$1.1 ps on the low frequency side and $\sim$2.7 ps on the high frequency side) in the amide I absorption spectrum.

[a)]Electronic mail: l.piatkowski@amolf.nl

I. INTRODUCTION

The amide motif (O=C–N–H) is extremely important in living systems as it forms the building block of the backbone of proteins. The structural dynamics of this backbone play a crucial role in the folding and functional conformational dynamics of proteins. These dynamics are very much dependent on the hydrogen-bond interactions among the amide moieties and their interactions with surrounding and solvating molecules like water[1,2].

An excellent system for studying the properties of the amide motif is N-methylacetamide (NMA). This molecule forms hydrogen bonds with other NMA molecules which mimic well the intra- and interchain hydrogen-bonding interactions of the backbones of proteins[3]. NMA has thus been widely used to investigate the properties of the amide motif in various molecular environments both experimentally[4–12] and theoretically[13–19].

The vibrational relaxation dynamics of the amide modes of NMA have been studied before with infrared vibrational spectroscopy[8,10,20–22] and with molecular dynamics simulations[16,17,23–27]. All previous studies of the vibrational dynamics of NMA showed that the amide vibrations relax via intramolecular energy transfer, irrespective of the solvent used. The highest frequency amide vibration, amide I, with a frequency of $\sim$1650 cm^{-1}, is always found to relax in two subsequent steps. The first step involves intramolecular energy transfer from the amide I mode to lower frequency amide modes, and the second step involves further redistribution of the vibrational energy among low frequency intra- and intermolecular modes, leading to a complete thermalization of the vibrational energy.

DeFlores *et.al.* studied the vibrational relaxation mechanism of NMA in D_2O and DMSO with two-dimensional vibrational spectroscopy[10]. In both solvents they observe a rapid energy exchange and equilibration between the amide I and the amide II modes upon broadband excitation of these modes. This rapid energy redistribution is followed by a much slower relaxation process that leads to thermalization of the vibrational energy. In our previous studies of hydrogen-bonded NMA clusters, we did not find any evidence of energy transfer between the amide I and amide II vibrations[28]. We observed that both the amide I and the amide II mode directly relax on a time scale $<$1 picosecond to lower-frequency intramolecular modes. So far no experimental work has been reported on the relaxation pathways of isolated non-bonded NMA molecules. Here we study the relaxation mechanisms of the amide I and amide II vibrations of isolated NMA molecules using polarization-resolved femtosecond two-color pump-probe spectroscopy.

II. EXPERIMENT

The polarization-resolved two-color pump-probe experiment employs femtosecond mid-infrared pulses that are generated by frequency conversion processes that are pumped with the near-infrared 800 nm pulses derived from a high energy Ti:Sapphire amplifier system. This system comprises a Coherent "Legend Duo" regenerative amplifier that delivers 40 fs pulses with a pulse energy of 7 mJ per pulse at a repetition rate of 1 kHz. We use about 6 mJ to pump an optical parametric amplifier (HE-TOPAS). The produced signal and idler pulses are used in a difference frequency mixing process in a silver gallium disulphide ($AgGaS_2$) crystal resulting in 60 μJ pulses with a central wavelength of $\sim$6000 nm ($\sim$1650 cm^{-1}), a pulse duration of $\sim$60 fs, and a spectral bandwidth of $\sim$400 cm^{-1}.

In the experiment a relatively narrow band pump pulse excites either the amide I (AI) or amide II (AII) vibration of NMA, thereby promoting the vibration from its ground state $\nu = 0$ to the first excited state $\nu = 1$. The narrow-band pump pulse is obtained by spectrally filtering the generated broadband infrared pump spectrum with a home-built Fabry-Pérot filter. This filter is an air spaced cavity that is created by two closely separated parallel semitransparent windows (reflectivity R = 90%). The Fabry Pérot filter transmits only the wavelengths that constructively interfere in the exit channel of the cavity. By changing the distance between the two windows we tune the transmitted beam wavelength and bandwidth. The thus obtained pump pulses have a bandwidth of $\sim$50 - 60 cm^{-1}, a pulse duration of $\sim$150 femtoseconds, and a pulse energy of $\sim$6 μJ (see figure 2).

The excitation of the amide mode results in ground-state depletion and stimulated emission $\nu = 1 \rightarrow 0$, thus leading to a decrease in absorption (bleaching) at frequencies corresponding to the $\nu = 0 \rightarrow 1$ transition. Simultaneously, the population of the $\nu = 1$ state leads to an induced absorption at frequencies corresponding to the ν=1$\rightarrow$2 transition. These transient changes in absorption are monitored with a second broadband infrared probe pulse.

The probe and reference beams are split off from the broadband infrared pulse beam using two wedged BaF_2 windows. The probe is sent into a 3 fs resolution delay stage. The pump and probe pulses are focussed to the same spot in the sample using a gold-coated parabolic mirror. The reference pulse is also focused in the sample by the same mirror, but not in overlap with the pump. After the sample, the probe and reference beams are dispersed with an Oriel monochromator and detected with an Infrared Associates 2$\times$32 pixels mercury-cadmium-telluride (MCT) detector

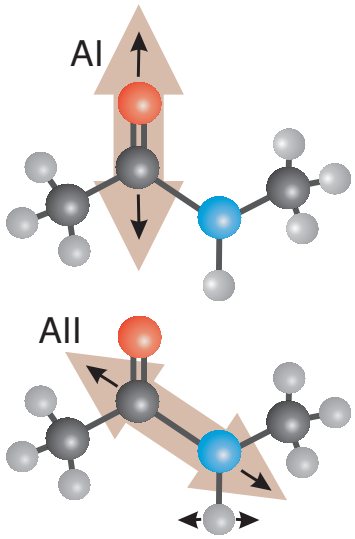

FIG. 1. Molecular structure of the trans-NMA molecule. The black arrows indicate the atomic motions associated with the amide I and amide II vibrations.

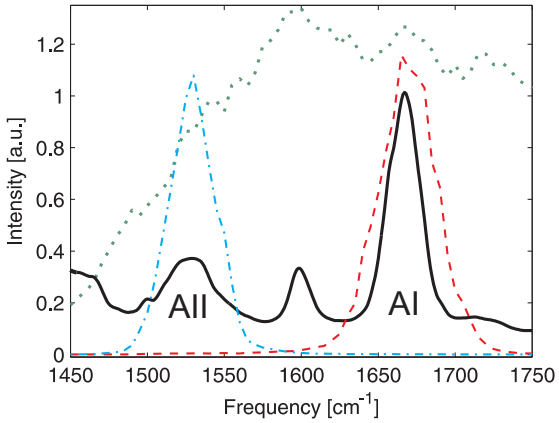

FIG. 2. Spectra of the probe pulse (dotted) and the two pump pulses used to excite either the amide I or amide II mode of the NMA molecule (dashed and dashed-dotted lines, respectively). The absorption spectrum of a 10 mM solution of NMA in $CHBr_3$ is represented by the solid line.

array. The reference allows for a frequency-resolved correction for shot-to-shot fluctuations of the probe-pulse energy.

Before entering the sample, the polarization of the probe is rotated to an angle of 45° with respect to the polarization of the narrow-band pump using a wire-grid polarizer. After the sample the polarization component parallel to the pump or the component perpendicular to the pump is selected using a polarizer mounted in a motorized rotation stage. The thus obtained transient

absorption changes $\Delta\alpha_{\parallel}(t,\nu)$ and $\Delta\alpha_{\perp}(t,\nu)$ are used to construct the so-called isotropic signal:

$$\Delta\alpha_{iso}(t,\nu) = \frac{\Delta\alpha_{\parallel}(t,\nu) + 2\cdot\Delta\alpha_{\perp}(t,\nu)}{3}\,, \tag{1}$$

which is not sensitive to depolarization of the excitation and gives information on the rate of vibrational energy relaxation and energy transfer.

The signals $\Delta\alpha_{\parallel}(t,\nu)$ and $\Delta\alpha_{\perp}(t,\nu)$ are also used to construct the so-called anisotropy parameter $R(t,\nu)$ that exclusively represents the dynamics of the depolarization of the excitation:

$$R(t,\nu) = \frac{\Delta\alpha_{\parallel}(t,\nu) - \Delta\alpha_{\perp}(t,\nu)}{3\cdot\Delta\alpha_{iso}(t,\nu)} \tag{2}$$

The anisotropy parameter $R(t,\nu)$ represents the normalized difference between parallel and perpendicular pump-probe polarizations. $R(t,\nu)$ is proportional to the second-order autocorrelation function of the direction of the transition dipole moment.[29]

The sample is a $\sim$10 mM solution (1:1000 molar ratio) of NMA in bromoform ($CHBr_3$). The advantage of using bromoform over carbontetrachloride is that there are no vibrational resonances overlapping with the amide modes. For highly diluted solutions the weak vibrational mode of CCl_4 at $\sim$1530 cm^{-1} overwhelms the AII absorption band. Bromoform possesses a weak absorption at $\sim$1600 cm^{-1} in between the absorption bands of the AI and AII modes. Hence, these amide modes can be excited without exciting the solvent molecules. The sample is contained in an infrared sample cell consisting of two 2 mm thick CaF_2 windows and a 1.2 mm thick teflon spacer.

III. RESULTS AND DISCUSSION

A. Linear spectra

NMA is dominantly present in its trans conformation, which means that the C=O and N-H groups reside at opposite sites of the C-N backbone bond of the molecule (see figure 1)[12,18]. Both the amide I and the amide II modes are combinations of local vibrations. The contributions of the different local vibrations to the amide normal modes of NMA have been determined with potential energy distribution calculations[5,6,16]. The amide I mode is dominated by the C=O stretch vibration ($\sim$80%), whereas the amide II mode is a combination of the C-N stretch and N-H bend vibrations, together accounting for nearly 70% of the vibrational amplitude.

In figure 2 we show the linear absorption spectrum of a solution of 10 mM NMA in bromoform ($CHBr_3$). The two amide modes are centered at $\sim$1665 cm^{-1} (AI) and $\sim$1535 cm^{-1} (AII). The

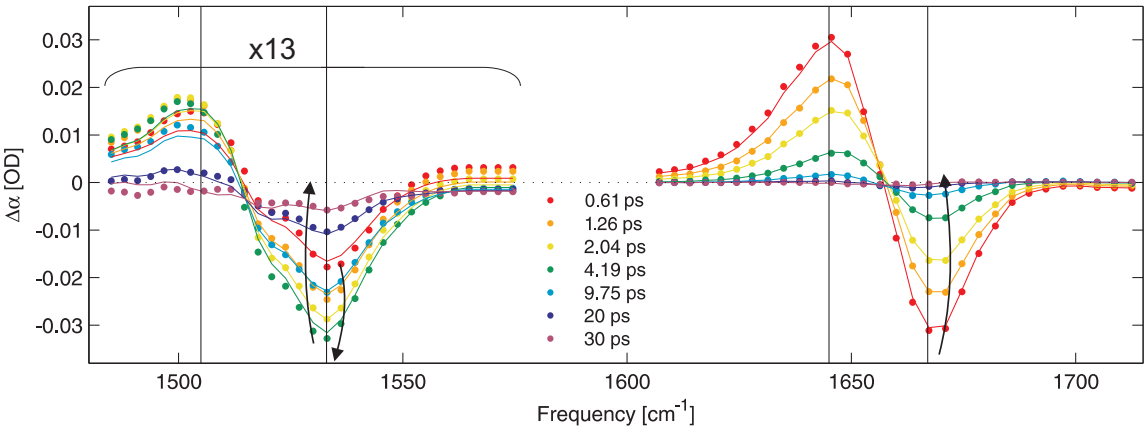

FIG. 3. Transient spectra in the frequency range of the AI and AII modes at different delay times following excitation of the AI mode of a 10 mM solution of NMA in $CHBr_3$. The solid lines represent the results of a fit to the relaxation model described in the text. For clarity, the response of the AII mode has been multiplied by a factor of 13. The arrows indicate the time evolution of the amplitude of the spectra.

small absorption band centered at 1600 cm^{-1} originates from the solvent. At this low concentration only trans-NMA monomers will be present in solution[12,15,18,28]. The AI absorption band is somewhat asymmetric with a shoulder on the lower frequency side. The AII band is weaker ($\sim$1/5) and somewhat broader than the AI band. The central frequency of the AI mode ($\sim$1670 cm^{-1}) is redshifted with respect to the central frequency of the AI mode of NMA dissolved in carbon tetrachloride ($\sim$1690 cm^{-1}) at the same concentration. This difference likely results from the dipole-dipole interaction between the NMA molecule and the small ($\sim 3 \cdot 10^{-30}$ [C·m]) dipole moments of the solvating bromoform molecules. The frequency splitting of the two amide modes is similar to that of hydrogen-bonded NMA clusters in CCl_4.

B. Vibrational energy relaxation

1. Exciting the amide I mode

Figure 3 shows transient absorption spectra in the frequency ranges of the AI and AII modes at different delay times after excitation of the AI mode. The spectral response in the AII region has been multiplied by a factor of 13 for clarity. Both the transient spectra of the AI and AII mode are characterized by a negative (bleach) contribution at high frequencies ($>$1515 and $>$1660 cm^{-1} respectively) representing the reduced absorption and stimulated emission of the $\nu = 0 \rightarrow 1$ transi-

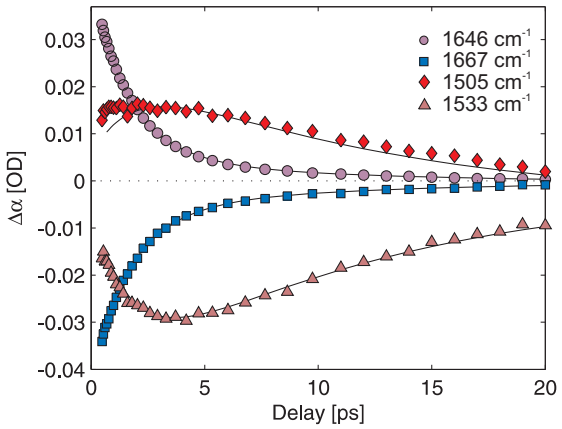

FIG. 4. Time traces recorded at four different frequencies corresponding to the maxima of the bleach and the induced absorption signals of the AI and AII modes. The frequencies are marked with solid vertical lines in figure 3. The solid black lines represent the results of a fit to the relaxation model described in the text.

tion, and a positive signal at lower frequencies ($<$1515 and $<$1660 cm^{-1}), representing the induced $\nu = 1 \rightarrow 2$ absorption. For the AI mode both the bleach and induced absorption decay in time. After $\sim$30 ps the transient spectrum is nearly zero and does not change anymore with delay time.

The spectral changes in the AII frequency region show very different dynamics from the AI frequency region. At early delay times, up to a delay time of $\sim$4 ps, the amplitude of the AII transient spectrum increases. For delays larger than $\sim$4 ps the signal slowly decays. After about 40 ps the transient spectrum does not change anymore. The induced absorption shows a much less pronounced ingrowth than the bleaching.

In figure 4 we show delay traces (circles/squares and diamonds/triangles correspond to AI and AII modes, respectively) that are recorded at the frequencies corresponding to the maxima of the bleach and the induced absorption signals of both amide modes. These frequencies are marked with black vertical lines in figure 3. It is clear that the dynamics of both modes is very different and involves at least two distinct regimes. The response of the AI mode shows a fast decay at early delays ($<$4 ps) and a much slower decay at later delays. The response of the AII mode is characterized by two similar rates, however, in contrary to the AI dynamics, the first fast process leads to an ingrowth of the intensity of the AII signal. This process is followed by a decay with the slower rate.

Upon close inspection of the spectral dynamics of the AI mode we observe a frequency de-

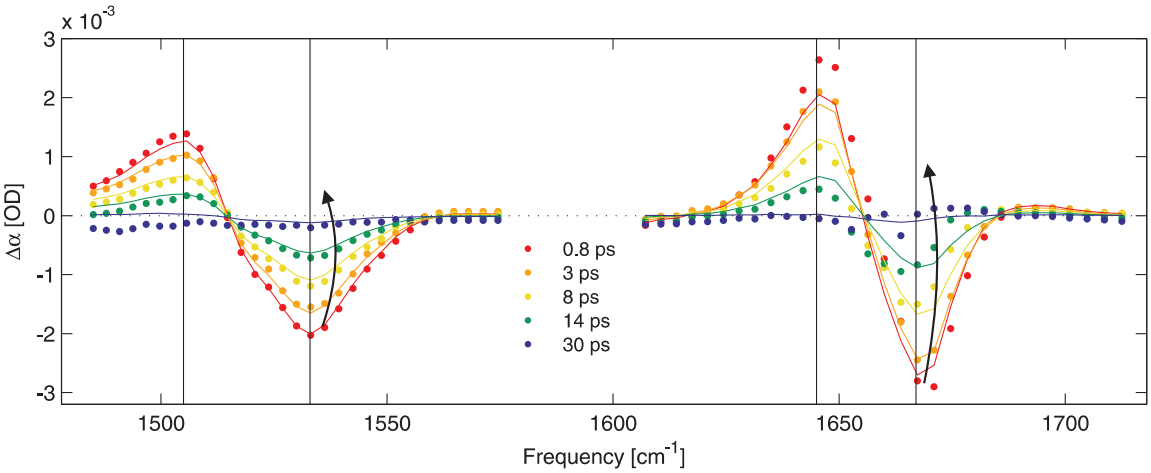

FIG. 5. Transient spectra at different delay times following excitation of the AII mode of a 10 mM solution of NMA in $CHBr_3$. The solid lines represent the results of a fit to the relaxation model described in the text. The black arrows indicate the time evolution of the amplitude of the spectra.

pendence of the decay. For delays $<$5 ps the signal in the blue wing of the AI transient spectrum decays slower than the signal in the red wing of the spectrum. The high frequency side of the transient spectrum decays with a time constant of $\sim$2 ps, whereas the low frequency side decays faster with a time constant of $\sim$1 ps. This variation in the dynamics across the AI transient spectrum leads to a transient blue shift of the AI spectral response (the red wing decays faster than the blue wing). At later delays this difference vanishes, the transient signal decays uniformly across the spectrum on a much slower time scale. We did not observe a similar spectral dependence of the dynamics in the AII frequency region.

2. Exciting the amide II mode

In figure 5 we show transient spectra recorded in the frequency range of the AI and AII modes for five delay times after excitation of the AII mode. Both the AI and AII responses consist of a negative absorption change on the high frequency side of the fundamental absorption band and a positive signal on the low frequency side, similar as was observed when the AI mode was excited. The AII and AI responses have their maximum intensity around 0 ps and both show a similar slow decay. After about 30 ps the transient spectrum does not change anymore, which implies that the system has reached thermal equilibrium.

Figure 6 shows time traces (circles/squares and diamonds/triangles correspond to AI and AII

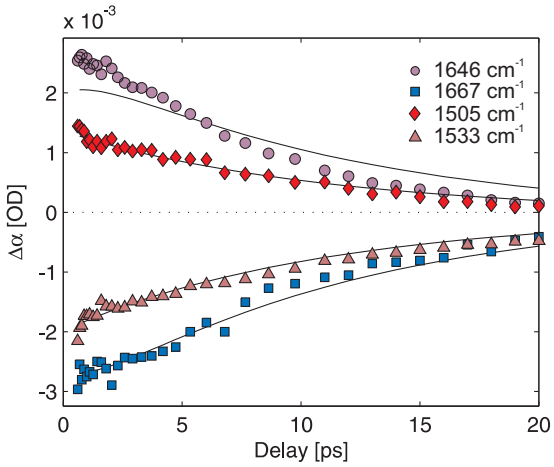

FIG. 6. Time traces recorded at four different frequencies corresponding to the maxima of the bleach and the induced absorption signals of the AI and AII modes following excitation of the AII mode. The solid lines result from a fit to the relaxation model described in the text.

mode respectively) at the four frequencies that are marked with solid black lines in figure 5. Clearly, the signals at the four different frequencies are very much alike, all showing a decay time constant of about 10 ps.

3. Interpretation and Modeling

The AI mode shows a fast decay that is faster in the red wing than in the blue wing of the absorption band. This observation indicates that the AI vibrational band contains different subbands with different vibrational relaxation rates. In previous experimental and theoretical work strong indications were found that the absorption band of the AI mode indeed contains two subbands[8,20]. Therefore we will model the vibrational relaxation dynamics with two AI $\nu = 1$ states with different vibrational relaxation time constants.

The excitation of the AI mode leads to a direct response in the frequency region of the AII mode. This observation indicates that the AI and AII mode are anharmonically coupled. This response consists of a bleaching in the blue wing of the AII absorption spectrum and an induced absorption in the red wing, which means that the excitation of the AI mode induces an anharmonic redshift of the AII mode. The transient spectrum of the AII mode resulting from this redshift shows a smaller frequency difference between the maxima of the bleach and the induced absorption than in case the AII mode is excited. Following this direct anharmonic response of the AII mode, we observe

a further ingrowth of the bleach and the induced absorption on a time scale that is similar to the time scale of the decay of the two AI subbands. The complimentary character of these dynamics indicates that the $\nu = 1$ states of the two subbands of the AI mode transfer their energy at least in part to the $\nu = 1$ state of the AII mode. This state constitutes a third level in the relaxation model.

If there is a coupling leading to energy transfer from the $\nu = 1$ states of the two AI subbands to the $\nu = 1$ state of AII, the same coupling will also lead to transfer of energy in the other direction, i.e. from the $\nu = 1$ state of AII to the $\nu = 1$ states of the two AI subbands. Because of detailed balance, the two rates differ by a Boltzmann factor which for the energy exchange between the $\nu = 1$ states of AI and AII (ΔE = $\sim$140 cm^{-1}) equals $\sim$0.5. The rate at which the energy is equilibrated between the two modes is the sum of the two rates, irrespective of which mode is excited in the first place. This means that the rapid decay observed for the two AI subbands cannot be due to energy transfer to AII because we do not observe a similar partial fast decay when the AII mode is excited. Figure 6 clearly shows that excitation of the $\nu = 1$ state of AII only leads to a slow relaxation on a time scale of $\sim$10 ps. Therefore, we conclude that that only a minor part of the excitation of the two AI subbands is transferred to AII. The dominant relaxation channel of the two AI subbands involves transfer of energy to combination tones of other lower-frequency (amide) vibrations. This final state is the fourth and final level of the relaxation and has a spectral response that is not very different from the response that is obtained after the energy of the excitation is fully equilibrated (thermalized)[9,19].

The excitation of the AII mode is observed to lead to a direct transient spectral response in the frequency regime of the AI mode, which shows that the AI and AII modes are anharmonically coupled, similar as was observed in the experiment in which the AI mode was excited. Both the responses in the frequency region of the AII and the AI mode decay on a timescale of about 10 ps. This decay is partly due to energy transfer to the $\nu = 1$ states of the two AI subbands and partly due to energy relaxation to combination tones of lower-frequency (amide) vibrations.

The complete relaxation model thus consists of four levels: two levels represent the $\nu = 1$ states of two AI subbands and account for the frequency dependence of the fast relaxation following excitation of the AI mode, the third level represents the $\nu = 1$ state of the AII mode and the fourth level represents the final thermal state. All levels have associated differential spectral responses (difference between the absorption spectrum starting from that level and the linear absorption spectrum) in the frequency regions of the AI and the AII modes. In modeling the data we assume that the spectral responses of the two AI excited states are the same in the frequency region of

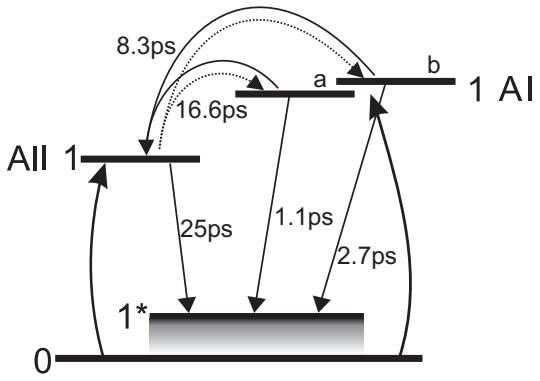

FIG. 7. Schematic representation of the relaxation model used in describing the relaxation pathways of the AI and AII modes in single NMA molecules upon excitation of either of the two modes.

the AII band, and we also assume that the rate the two AI subbands show the same rate of energy to the AII mode. The relaxation model is illustrated in figure 7. We fit all measurement results simultaneously to this relaxation model in a global fit. The results of this fit are represented in figures 3, 4, 5 and 6 by the solid lines.

From the fit we obtain the differential spectra associated with each of the levels, as shown in figure 8, and the relaxation time constants that connect the states of the relaxation model. The differential spectra associated with two AI excited states are represented by the blue and green spectra in figure 8. The spectra show a strong bleaching and induced absorption in the frequency region of the AI mode that are similar in shape for the two levels but shifted by $\sim$10 cm^{-1} with respect to each other. The response of the two excited AI levels in the frequency region of the AII mode is clearly upshifted with respect to $\Delta\alpha$=0 and differs from the usual antisymmetric differential spectral shape that results from an anharmonic frequency shift. The upshift probably results from the presence of a long low-frequency tail of the $\nu = 1 \rightarrow 2$ induced absorption of the excited AI subbands. The total transient spectral response in the frequency region of the AII mode is thus the sum of this low-frequency tail and an antisymmetric signal due to the anharmonic shift of the AII mode induced by the excitation of the AI subbands. Both contributions decay when the AI subbands relax. The level associated with the $\nu = 1$ state of the lower-frequency AI subband decays with a time constant $T_{1,AIa}$ of 1.1$\pm$0.1 ps to the final (thermal) level, and the level associated with the higher-frequency AI subband decays with a time constant $T_{1,AIb}$ of 2.7$\pm$0.4 ps. In addition to these relaxation channels, both AI subbands transfer energy to the AII level with a time constant of 8.3$\pm$1 ps.

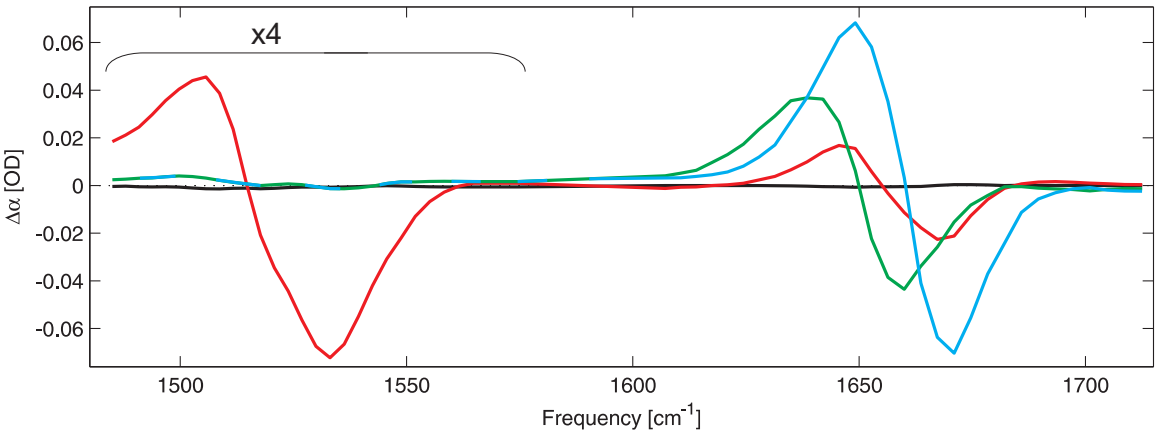

FIG. 8. Extracted differential spectra corresponding to the excited states of the AI mode (blue and green), the excited state of the AII mode (red), and the thermally equilibrated state (black).

The differential spectrum associated with the $\nu = 1$ state of the AII state is represented by the red line. This differential spectrum consists of a strong $\nu = 0 \rightarrow 1$ bleaching and $\nu = 1 \rightarrow 2$ induced absorption in the AII frequency region, and a much weaker bleaching and induced absorption in the frequency region of the AI mode. The latter differential spectral response represents the anharmonic redshift of the two AI subbands due to the excitation of the AII mode. The $\nu = 0 \rightarrow 1$ bleaching and $\nu = 1 \rightarrow 2$ induced absorption of the AII mode have a much larger amplitude than the differential spectrum that results from the anharmonic shift induced by the excitation of the two AI subbands. Therefore, the energy transfer from the two AI subbands to AII leads to an ingrowth of the signal in the AII frequency region. The $\nu = 1$ state of the AII mode decays both as a result of energy transfer to the two AI subbands with a time constant of 16.6$\pm$2 ps, and because of relaxation to the final (thermal) state with a time constant of 25$\pm$5 ps. The two relaxation channels together explain the observed relaxation time scale of $\sim$10 ps.

The differential spectrum of the final thermalized state is represented by the black line. This differential spectrum has very little amplitude in both the frequency regions of AI and AII. Therefore the relaxation to the final thermal state leads to a decay of the responses in both the AI and the AII frequency regions.

4. Anisotropy

From the two recorded signals $\Delta\alpha_{\parallel}$ and $\Delta\alpha_{\perp}$ we constructed the anisotropy parameter $R(\mathrm{t})$. In figure 9 we show the anisotropy decay for the AI mode (open circles) and for the AII mode

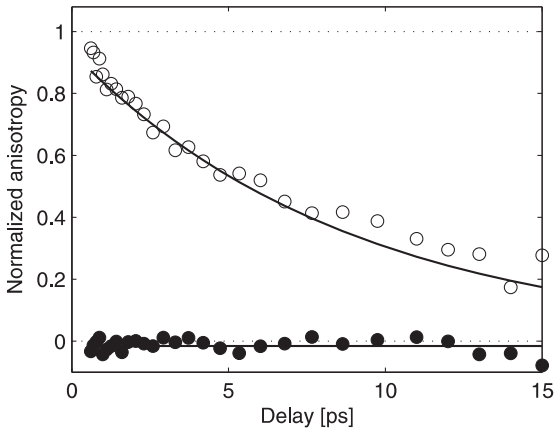

FIG. 9. Anisotropy time traces of the AI mode (open circles) and the AII mode (solid circles) after excitation of the AI mode. The solid lines represent an exponential function fitted to the AI mode anisotropy, and a constant value for the anisotropy of the AII mode.

(black circles) following excitation of the AI mode. The anisotropy of the AI mode decays with a time constant τ_{or} of 9$\pm$1 ps, which reflects the time scale of the reorientation of this vibration. The initial value of the anisotropy of the AII mode reflects the relative orientation of the transition dipole moment of the AII mode with respect to that of the excited AI mode. Using the following equation:

$$R(\nu,\theta) = \frac{1}{5}(3\cos(\theta)^2 - 1)\,, \tag{3}$$

which relates the relative angle θ between the excited and unexcited modes and the initial anisotropy value $R(\nu,\theta)$ for the mode to which the vibrational energy is transferred, we find an angle of $\sim$55°. This value is the same as the one found in our previous studies of hydrogen-bonded NMA clusters[28].

C. Discussion

The relaxation dynamics observed for NMA monomers strongly differ from the relaxation behavior observed for hydrogen-bonded NMA clusters[28]. In the first place the relaxation of the AI mode and in particular of the AII mode is much faster for the clusters than for the monomers (0.85 and 0.6 ps versus $\sim$1.5 ps and $\sim$10 ps). It thus appears that the presence of hydrogen bonds between the NMA monomers leads to a strong acceleration of the vibrational relaxation. This acceleration can be due to the fact that the hydrogen bonds take up part of the vibrational en-

ergy, thereby compensating for the energy mismatch between the excited vibration and the energy accepting combination tones of lower frequency vibrations.

An interesting difference between the relaxation behavior of the monomers and the clusters is that for the monomers we observe a partial relaxation of the excited $\nu = 1$ state of the two AI subbands to the $\nu = 1$ state of the AII mode. The energy transfer from AI to AII leads to a rise of the response of the AII spectral response on a time scale that is much shorter than the characteristic time scale of the energy transfer of $\sim$8 ps, and that corresponds to the vibrational relaxation time of the two AI subbands. The time scale of the vibrational relaxation of the AI modes is observed in the ingrowth of the AII response because the AI modes can no longer further populate the AII mode after they have relaxed. In a molecular dynamics study by Bloem *et.al.* evidence was found for a direct transfer between AI and AII, but on a time scale that is $\sim$10 times shorter than we observed[17]. The observation of energy transfer between the excited AI and AII vibrations does not agree with the theoretical results of Zhang *et.al.*[16] who found that for isolated NMA molecules the AII mode does not participate in vibrational relaxation of the AI mode. It should be noted at this point that we find the fraction of NMA molecules for which the two AI subbands relax via the AII mode to be quite small. From the rate constants we derive that this fraction is [0.12/(0.12+0.90)+0.12/(0.12+0.37)]/2 = 0.18. Hence, for less than 20% of the NMA molecules the AI model relaxes via energy transfer to the AII mode. For the NMA clusters, the direct vibrational relaxation of AI and AII is faster, and thus the fraction of NMA molecules showing energy transfer between AI and AII may become even smaller, which may explain why for the NMA clusters this process is not observed[28].

The vibrational lifetime of the AI mode is observed to be frequency dependent. NMA molecules absorbing on the high frequency side ($\sim$1680 cm^{-1}) relax slower than molecules absorbing in the red wing of the spectrum ($\sim$1660 cm^{-1}). One possible explanation for this observation is that the NMA spectrum is inhomogeneously broadened due to a variation in conformation. Previous molecular dynamics simulations showed that the trans-NMA molecule can exist in four conformations of planar symmetry with different orientations of the C- and N- methyl groups[6]. If this variation in conformation would be the origin of the frequency dependence of the vibrational lifetime, one would expect the lifetime to vary continuously over the AI absorption band. In that case one would also expect a frequency dependence in the vibrational lifetime of the AII mode of NMA. However, for the AII mode we do not observe such a frequency dependence.

We find that a relaxation model involving only two different rates is fully sufficient to de-

scribe the experimental data at all delay times. This finding agrees with the results of a previous experimental study[8] and with the results of molecular dynamics simulations[20]. Rubtsov *et.al.*[8] investigated the coupling between different amide modes of small peptides dissolved in chloroform with two-dimensional infrared spectroscopy. They found strong indications for the presence of two subbands in the spectrum of the AI mode, both in the linear absorption spectrum and in the transient nonlinear vibrational response. They attributed the two subbands to the splitting of the AI mode by a Fermi resonance of this mode with an overtone of a lower-frequency vibration. DeCamp *et.al.*[20] performed molecular dynamics simulations on solutions of NMA in $CDCl_3$, and they attributed the presence of two subbands to a difference in the number of hydrogen bonds formed between NMA and $CDCl_3$ solvent molecules. They found that singly hydrogen-bonded NMA molecules absorb at the high-frequency side of the absorption spectrum, and that doubly hydrogen-bonded NMA molecules absorb at the red side of the absorption band. Figure 2 shows that the linear absorption spectrum of the AI mode of NMA in $CHBr_3$ possesses a shoulder on the low-frequency side. Interestingly, this shoulder is not present in the linear absorption spectrum of the AI mode for a solution of 10 mM NMA in CCl_4 solution[28]. This result suggests that the shoulder arises from NMA molecules interacting with $CHBr_3$ solvent molecules, in line with the explanation of DeCamp *et.al.*.

We observed that the transition dipole moments of the AI and AII modes of NMA monomers have the same relative angle of $\sim$55° as we observed previously for hydrogen-bonded NMA clusters. This angle is consistent with the findings of previous experimental studies[10]. Apparently, the hydrogen-bond interactions between the NMA molecules have very little effect on the normal mode character and thus the direction of the transition dipole moment of the AI and AII vibrations. The reorientation time τ_{or}=9$\pm$1 ps and is comparable with the time constant found by DeCamp et. al.[20] for NMA dissolved in D_2O and $CDCl_3$ and with the time constant by Hamm et. al. for deuterated NMA dissolved in D_2O[21]. The reorientation time constant of $\sim$9 ps is somewhat longer than the reorientation time constant of 6 ps that we observed for hydrogen-bonded NMA clusters in CCl_4. This result may seem surprising as one would expect that single NMA molecules reorient faster than NMA oligomers. One reason for this unexpected result may be the difference in viscosity of the solvent. The viscosity of bromoform is approximately twice as high ($\sim$1.85 mPa·s) than that of carbon tetrachloride ($\sim$0.97 mPa·s). According to hydrodynamic theory[30] the reorientation time constant is proportional to the viscosity of the solvent: $\tau_{or}=V\eta/k_BT$, with V the volume of the solute, η the viscosity, k_B Boltzmann's constant, and T the temperature. Even so, it remains

surprising that the effective larger volume of an NMA cluster in comparison to an NMA monomer does not lead to a strong increase of the reorientation time constant of the AI mode. A possible reason for the relatively fast decay of the anisotropy for the NMA clusters is that the anisotropy can also decay as a result of vibrational resonant energy transfer between the excited and unexcited amide modes within the hydrogen-bonded cluster.

IV. CONCLUSIONS

We studied the vibrational energy relaxation mechanisms of the amide I and amide II vibrations of monomeric N-methylacetamide (NMA) molecules dissolved in bromoform using polarization-resolved femtosecond two-color pump-probe spectroscopy. We excited both the amide I and the amide II vibration to the $\nu = 1$ excited state with a narrow-band mid-infrared pump pulse with a pulse duration of $\sim$150 femtoseconds, and we monitored the vibrational relaxation in the frequency regions of both modes with a short, broadband mid-infrared probe pulse with a pulse duration of $\sim$60 femtoseconds.

We observe that the vibrational relaxation of the amide I mode depends on frequency. This frequency dependence can be well explained from the presence of two subbands with different vibrational lifetimes in the absorption spectrum of the amide I mode. The presence of two subbands agrees with the observation of a low-frequency shoulder in the linear absorption spectrum of the amide I mode. The two subbands are likely caused by a difference in the interaction strength of NMA with the bromoform solvent molecules.

We find that the excited amide I mode relaxes via two vibrational relaxation channels. In one channel the vibration relaxes to a final state with an absorption spectrum that corresponds to a full equilibration of the vibrational excitation energy. The time constants for this relaxation are found to be 1.1$\pm$0.1 ps for the subband at the red side of the amide I absorption band and 2.7$\pm$0.4 ps for the subband at the blue side of the amide I absorption band. In the other channel the two subbands transfer their energy to the $\nu = 1$ state of the amide II mode. This process has a much longer time constant of 8.3$\pm$1 ps, which implies that only for $\sim$20% of the NMA molecules the amide I mode relaxes via energy transfer to the amide II mode. The excited amide II mode relaxes via two similar relaxation channels, i.e. via relaxation to a final thermalized state with a time constant of 25$\pm$5 ps, and via energy transfer to the amide I mode with a time constant of 16.6$\pm$2 ps.

ACKNOWLEDGMENTS

The work is part of the research program of the Foundation for Fundamental Research on Matter (FOM) which is financially supported by the Dutch organization for Scientific Research (NWO). The authors would like to thank Hinco Schoenmaker for technical support.

REFERENCES

[1]S. K. Pal and A. H. Zewail, *Chem. Rev.* **104**, 2099–2123 (2004).

[2]S. K. Pal, J. Peon, and A. H. Zewail, *PNAS* **99**, 1763–1768 (2002).

[3]T. W. Whitfield, G. J. Martyna, S. Allison, S. P. Bates, H. Vass, and J. Crain, *J. Phys. Chem. B* **110**, 3624–3637 (2006).

[4]Y. Liu, M. A. Czarnecki, and Y. Ozaki, *Appl. Spec.* **48**, 1095 (1994).

[5]W. A. Herrebout, K. Clou, and H. O. Desseyn, *J. Phys. Chem. A* **105**, 4865 (2001).

[6]X. Chen, R. Schweitzer-Stenner, S. Asher, N. Mirkin, and S. Krimm, *J. Phys. Chem.* **99**, 3074–3083 (1995).

[7]I. Noda, Y. Liu, and Y. Ozaki, *J. Phys. Chem.* **100**, 8665–8673 (1996).

[8]I. V. Rubtsov, J. P. Wang, and R. M. Hochstrasser, *J. Phys. Chem. A* **107**, 3384–3396 (2003).

[9]H. Huang, S. Malkov, M. Coleman, and P. Painter, *J. Phys. Chem. A* **107**, 7697–7703 (2003).

[10]L. P. DeFlores, Z. Ganim, S. F. Ackley, H. S. Chung, and A. Tokmakoff, *J. Phys. Chem. B* **110**, 18973–18980 (2006).

[11]M. M. Omar, *J. Chem. Soc. Faraday Trans.* **76**, 711–716 (1980).

[12]K. Pralat, J. Jadzyn, and S. Balanicka, *J. Phys. Chem.* **87**, 1385 (1983).

[13]H. Torii, T. Tatsumi, T. Kanazawa, and M. Tasumi, *J. Phys. Chem. B* **102**, 309–314 (1997).

[14]X. N. Jiang and C. S. Wang, *Chem. Phys. Chem.* **10**, 3330–3336 (2009).

[15]M. Akiyama and H. Torii, *Spec. Chim. Acta A. Mol. Bio.* **56**, 137 (1999).

[16]Y. Zhang, H. Fujisaki, and J. E. Straub, *J. Phys. Chem. A* **113**, 3051–3060 (2009).

[17]R. Bloem, A. G. Dijkstra, T. l. C. Jansen, and J. Knoester, *J. Chem. Phys.* **129**, 055101 (2008).

[18]T. Miyazawa, T. Shimanouchi, and S. I. Mizushima, *J. Chem. Phys.* **29**, 611 (1958).

[19]R. Ludwig, O. Reis, R. Winter, F. Weinhold, and T. C. Farrar, *J. Phys. Chem. B* **102**, 9312–9318 (1998).

[20]M. F. DeCamp, L. DeFlores, J. M. McCracken, A. Tokmakoff, K. Kwac, and M. Cho, *J. Phys. Chem. B* **109**, 11016–11026 (2005).

[21]P. Hamm, M. Lim, and R. M. Hochstrasser, *J. Phys. Chem. B* **102**, 6123–6138 (1998).

[22]S. Woutersen, Y. Mu, G. Stock, and P. Hamm, *Chem. Phys.* **266**, 137 (2001).

[23]K. Kwac and M. Cho, **36**, 326 (2005).

[24]H. Torii, *J. Phys. Chem. A* **110**, 4822–4832 (2006).

[25]A. G. Dijkstra, T. I. C. Jansen, R. Bloem, and J. Knoester, *J. Chem. Phys.* **127**, 194505 (2007).

[26]P. H. Nguyen and G. Stock, *J. Chem. Phys.* **119**, 11350 (2003).

[27]A. Bastida, M. A. Soler, J. Zúñiga, A. Requena, A. Kalstein, and S. Fernández-Alberti, *J. Chem. Phys.* **132**, 224501 (2010).

[28]L. Piatkowski and H. J. Bakker, *J. Phys. Chem. A* **114**, 11462–11470 (2010).

[29]H. Graener, G. Seifert, and A. Laubereau, *Chem. Phys.* **175**, 193–204 (1993).

[30]D. R. Bauer, J. I. Brauman, and R. Pecora, *J. Am. Chem. Soc.* **96**, 22 (1974).